Open Ceramics 19 (2024) 100655

Contents lists available at ScienceDirect

Open Ceramics

journal homepage: www.sciencedirect.com/journal/open-ceramics

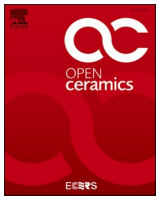

Linear volumetric additive manufacturing of zirconia from a transparent photopolymerizable ceramic slurry via Xolography

J.C. Sänger [a,b,*], N.F. König [c], A. De Marzi [d], A. Zocca [b], G. Franchin [d], R. Bermejo [a,e], P. Colombo [d,e], J. Günster [b,f]

[a] Department of Materials Science, Montanuniversität Leoben, Leoben, Austria
[b] Federal Institute for Materials Research and Testing (BAM), Berlin, Germany
[c] xolo GmbH, Berlin, Germany
[d] Department of Industrial Engineering, University of Padova, Padova, Italy
[e] Departmentof Materials Science and Engineering, The Pennsylvania State University, USA
[f] Institute of Non-Metallic Materials, Clausthal University of Technology, Clausthal-Zellerfeld, Germany

ARTICLE INFO

Handling Editor: Dr Catherine Elissalde

Keywords:
Xolography
Additive manufacturing
Zirconia

ABSTRACT

Advanced ceramics printed with photon-based additive manufacturing deals with anisotropic mechanical properties from the layer-by-layer manufacturing. Motivated by the success in using highly filled transparent slurries containing nanoparticles for powder-based two-photon-polymerization (2PP) for advanced ceramic printing, this works approach is the transfer to Xolography, a volumetric additive manufacturing technology based on linear two-photon excitation and without recoating steps. This paper reports the results of a preliminary investigation optimizing the photocurable slurry to the requirements of Xolography in terms of transparency, over a significantly larger mean free path, compared to 2PP. A feedstock filled with 70 % weight fraction of ceramic particles (~30 vol%) exhibiting an exceptionally high degree of transparency in the relevant wavelength range of 400–800 nm was prepared from 5 nm zirconia nanoparticles. The high transparency of the photocurable slurry is attributed to the near-monomodal particle size distribution of the zirconia nanoparticles used.

1. Introduction

Additive manufacturing (AM) of technical ceramics relies on powder-based processing routes to achieve parts possessing ceramic-typic mechanical, chemical, electrical and optical properties at all manufacturing scales. Vat Photo-Polymerization (VPP) technologies [1] promise high accuracy and are adapted to water-based [2] and organic slurries [3,4] highly filled with a wide range of ceramic particles from Alumina [2,4,5], Zirconia [6,7] and Piezo-ceramics [8] to Nitrides [3,9]. Lithography-based Ceramic Manufacturing (LCM) [10] currently offers a wide range of applicable ceramic slurries. These light-based printing technologies need to deal with the light scattering by ceramic particles in the organic photocurable resins. An accurate but time-consuming layer-by-layer recoating of thin slurry layers can compensate low curing depths and inaccuracies from light scattering [11,12] in single beam Stereolithography (SLA) or Digital Light Processing (DLP).

For AM of ceramics [1], Volumetric Additive Manufacturing is particularly interesting, as filigree structures can be generated avoiding the formation of interfaces between adjacent layers, in contrast to conventional layer-by-layer approaches, This should lead to stronger ceramic parts, as the interface between the layers acts as a source of defects, reducing the reliability of the material [13,14]. Moreover, complex components such as a ball-in-a-cage, can be directly obtained without the use of sacrificial supports. Recently, it has been shown that SiOC ceramics can be produced by the use of photocurable solutions containing transparent preceramic polymers in Xolography [15]. The respective use of colloidal silica particles has also been achieved to demonstrate silica glass printing, using computed axial lithography [16,17]. Volumetric particle loadings from 18 to 40 % were used, but it should be pointed out that silica has a refractive index rather similar to that of the photocurable liquid mixture. Indeed, to fabricate components based on a technical ceramic like zirconia with high three-dimensional resolution using volumetric additive manufacturing technologies, the optical properties of the slurries, mainly a high transparency, is pivotal. By utilizing ultra-fine and highly dispersed 5 nm nanoparticles it was demonstrated that light scattering of the slurries could be vastly

* Corresponding author. Federal Institute for Materials Research and Testing (BAM), Berlin, Germany.
E-mail address: johanna.saenger@bam.de (J.C. Sänger).

https://doi.org/10.1016/j.oceram.2024.100655
Received 31 January 2024; Received in revised form 13 June 2024; Accepted 6 August 2024
Available online 10 August 2024

reduced. This rendered fabrication by two-photon-polymerization (2PP) feasible, which had previously not been possible due to the severe light scattering in particle-containing conventional ceramic slurries [18]. Yttria stabilized zirconia (YSZ) ceramic structures with an unmatched resolution of 500 nm and outstanding mechanical properties were obtained [18,19]. 2PP possesses the highest volumetric resolution and accuracy of all technologies, but also the lowest build-up rate and the smallest printing envelope. Higher building rates are obtained with holographic [20] and tomographic [16,17] imaging technologies. These technologies use one excitation wavelength and therefore rely on conventional photoinitiators. Localization of the polymerization is achieved by balancing activating light dose and chemical inhibition.

The present study follows the concept of transparent nano sized particle filled resins and aims at transferring it to the Xolography technology, recently developed for acrylic photopolymers by xolo GmbH, Berlin, Germany [21]. Xolography is a linear volumetric AM technology, which relies on novel dual-color photoinitiators. These molecules are typically activated by UV light, in this setup provided by a 405 nm laser beam within a thin light sheet, inducing an efficient photoisomerization leading to another ground-state species characterized by high absorbance in the visible range of the electromagnetic spectrum. A visible light projection (450–650 nm) focused on this UV light sheet can selectively excite the activated photoinitiator molecules which results in localized photopolymerization inside a confined monomer volume. With a mean lifetime of a few seconds, the activated photoinitiator is deactivated by a thermal isomerization back to the initial state. By continuously moving the activating UV light sheet through the photopolymerizable resin and focusing with visible light a video projection on it, free-form structures can be directly inscribed into the volume of the liquid resin, avoiding the time-consuming feedstock dispersion in a layer-by-layer process intrinsic to most common AM-technologies. This fact also offers the possibility for continuous processing and up-scaling [22], as the printed parts are not connected to any sort of base plate or stage. On the contrary, attaching structures purposely to the cuvette walls allows precise positioning after e.g. a first washing step. In this way multiple resins can be processed inside the same cuvette enabling multimaterial AM [23]. For more details on the Xolography technology see Ref. [21].

Generally, ceramic materials offer a wide optical window of transparency, typically ranging from a wavelength below 0.3 μm–5 μm [24,25]. Yet, the optical properties of ceramic suspensions are governed by light scattering [26,27]. Predicting their optical properties requires a precise knowledge of the complex index of refraction $\tilde{n} = n + iK$ of the ceramic material and the liquid phase, where $\tilde{n}$ is depending on the optical constants n (refractive index) and K (extinction coefficient). In the case of ceramic suspensions, scattering takes place at the interface between the liquid phase and powder particles, according to the difference in refractive index. Absorption can occur within both the ceramic material and the liquid phase, and is expressed by K, i.e., the imaginary part of $\tilde{n}$. K is a material constant and indicates the amount of the absorption loss when an electromagnetic wave propagates through a material. K is directly proportional to the absorption coefficient α in Lambert-Beer's law of absorption $I(x) = I_0 \exp(-\alpha x)$, with I_0 the intensity of the incident light and I(x) the intensity of the light after passing a given length x through the material. Typically, K, α and n depend on the wavelength of the incident light. For a successful application of Xolography to ceramic suspensions, a high transmissivity at about 400–800 nm is mandatory, requiring low K at this wavelength range. Pure zirconia single crystals have a high transparency between 260 and 700 nm and therefore they should be suitable for Xolography [28]. However, even when K is close to zero and light absorption is negligible, the interaction of light with a ceramic suspension is still affected by scattering. In this case, the corresponding real part of $\tilde{n}$ of the ceramic material and the liquid phase, and the particle size are the critical parameters.

For particle sizes significantly larger than the wavelength of the interacting light, scattering is governed by classical optics [29]. According to Fresnel's formulas the difference in n of the ceramic material (for zirconia $n = 2.2$) and the liquid phase of the resin, comprised of monomer, solvent, photoinitiator, etc. ($n < 1.5$) results in a significant reflection at the interface between the ceramic particles and the liquid phase. For particle sizes in the range of the wavelength of the interacting light, light scattering is described by the MIE theory [26] and entire particles can be considered as individual scattering centers [27,30]. For both particle size regimes, the mean free path of photons in the volume of ceramic suspensions strongly depends on the ceramic particle packing density. For high solid loadings, as required for AM of ceramics, the mean free path is in the range of the wavelength of the incident light, even when the ceramic material absorption coefficient is close to zero. On the other hand, particles about ten times smaller than the wavelength of the interacting light are not recognized as individual scattering centers by the incident electromagnetic wave. Only their concentration affects the refractive index of the suspension by averaging the volume percentages weighted according to the respective refractive indices. Consequently, in this particle size regime, transmission of light through a ceramic suspension is possible.

The present communication is taking advantage of this fact, as already demonstrated for 2PP, and by the preparation of ceramic suspensions utilizing commercially available zirconia nanoparticles with a size of 5 nm, concentrated feedstocks exhibiting an exceptionally high degree of transparency in the relevant wavelength range of 400–800 nm. A possible synthesis route for them is described in Ref. [31].

2. Experimental

2.1. Material preparation

The photocurable feedstock for the Xolography process contained diurethane dimethacrylate (UDMA; CAS: 72869-86-4; Genomer 4247 by Rahn) and 4-acryloylmorpholine (ACMO, Rahn) which acts as reactive co-monomer and strengthens the polymer network (Sigma–Aldrich). 70 wt% of tetragonal zirconia nanoparticles dispersed in ethyl acetate (V-10-D, nanoBinder, CeraNovis GmbH, Saarbrücken, Germany) were added to the polymer followed by vacuum assisted solvent removal. 1 wt % related to the polymer content of each camphor (96 %, Sigma-Aldrich) and Triton™ X-100 (laboratory grade, Sigma Aldrich) were added to facilitate degassing during debinding and to adjust the dispersing agent to an organic matrix. 4-methoxyphenol (MEHQ, 99 %, Sigma-Aldrich) was added at 0.05 to 0.1 wt% as inhibitor to prevent uncontrolled polymerization caused by catalysis at the nanoparticle sites. 0.3 wt% photoinitiator (XC-471, xolo GmbH) was dissolved in N-methyldiethanolamine (MDEA, ≥99 %, Sigma-Aldrich). Furthermore, yttria-stabilized zirconia (YSZ, 3mol% yttria) suspensions with a larger size distribution were also investigated (nanoBinder, CeraNovis GmbH). In the following, the feedstocks for Xolography will be denoted as resins. From a ceramics processing point of view, they could also be denoted as slurries or suspension, but the term resin appears more appropriate considering their use as a photocurable system. The composition of the resins is reported in Table 1. For homogenization, the resin was mixed at different stages in a Hauschild SpeedMixer® DAC 600.2 VAC-P dual asymmetric centrifuge mixer.

2.2. Xolography printing setup

The resin was placed inside a single use UV-transparent cuvette (Brand GmbH) with base size of 10×10 mm^2 and a height of 35 mm and centrifuged to eliminate gas bubbles. The CAD models were sliced at 5 μm slice thickness and processed to print files using the software *xolid* from Xolo GmbH.

While the intensity of the visible light projection is set to its maximum per default, untested photopolymer formulations require careful screening of optimal print parameters in terms of printing speed,

Table 1
Composition of the resin employed with Xolography.

Chemical	Weight Fraction [wt%]	Volume Fraction [vol%]
V-10-D	50–70	70 wt% = 30 vol %
UDMA + ACMO	20-30 (ACMO:UDMA = 1:10)	Ca. 60
Camphor	1 related to UDMA + ACMO (100 mg/ml suspension in isopropanol)	
MEHQ	0.05–0.1 related to UDMA + ACMO (100 mg/ml suspension in isopropanol)	
XC 471	0.01–0.015 related to UDMA + ACMO (5 mg/1.666 g MDEA)	
MDEA	1-5 related to UDMA + ACMO	3–4

i.e., the forward movement of the UV light sheet, and the UV laser diodes' intensity or, more meaningful to the initiation of polymerization, their energy dose.

Print speeds between 0.5 mm/min and 5 mm/min were tested by printing small test plates of 1 mm thickness in the printing direction (see Fig. 4B), varying the UV energy dose. This parameter is given in mJ/mm^2 and reflects the amount of UV photons within the light sheet (approximating it as 2D, being a plane) penetrating through the vat during the print. Some energy doses are too low to generate enough activated photoinitiator, and thus no starting radicals are available for crosslinking and solidifying the resin. Then there is a range of energy doses that is just adequate to generate enough starting radicals for a controlled polymerization. At very high UV doses, undesired over-polymerization is observed. For the resins investigated, an optimal parameter set was determined to be at a speed of 2–3 mm/min and an UV energy dose of 8–10 mJ/mm^2. Printed structures were carefully extracted from the cuvettes and washed using a mixture of isopropanol (>99.5 %, Sigma–Aldrich) and tri(propylenglycol)methylether (Formlabs Inc.) to remove uncured material and were later postcured for 6

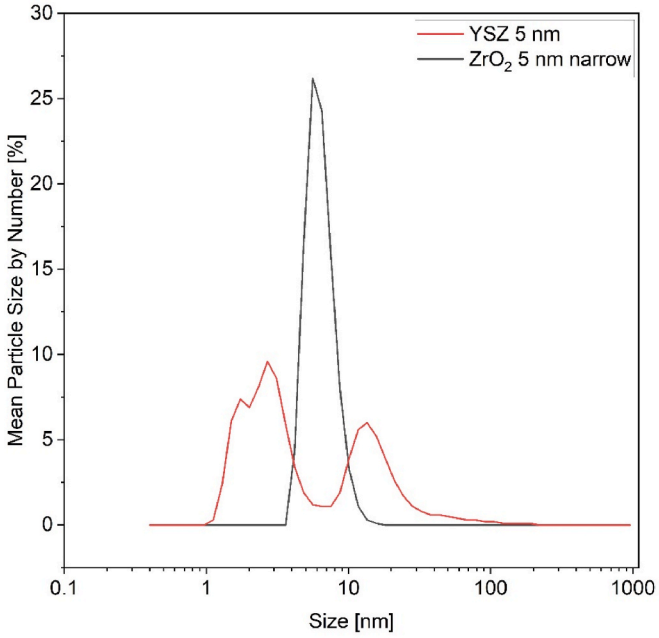

Fig. 2. A) Mean particle size by number of a YSZ suspension with mean particle size of 5 nm as used for 2PP, and of an improved ZrO_2 suspension with a narrow particle size distribution of 5 nm.

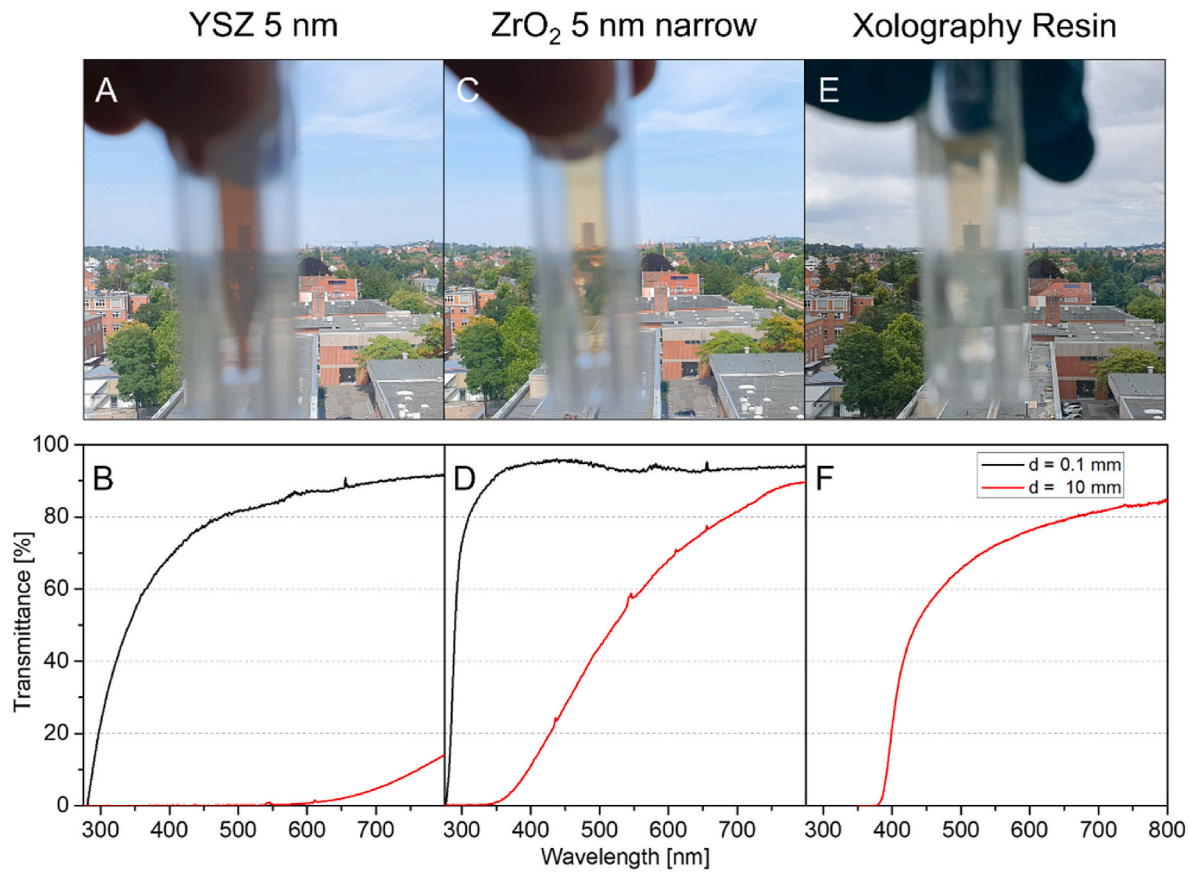

Fig. 1. Photos through a 10 mm micro cuvette and transmission curves of 0.1 and 10 mm through the respective suspensions of: A,B) 45 wt% YSZ suspension used for 2PP and C, D) 40 wt% ZrO_2 suspension with narrow particle size distribution. E, F) Xolography resin.

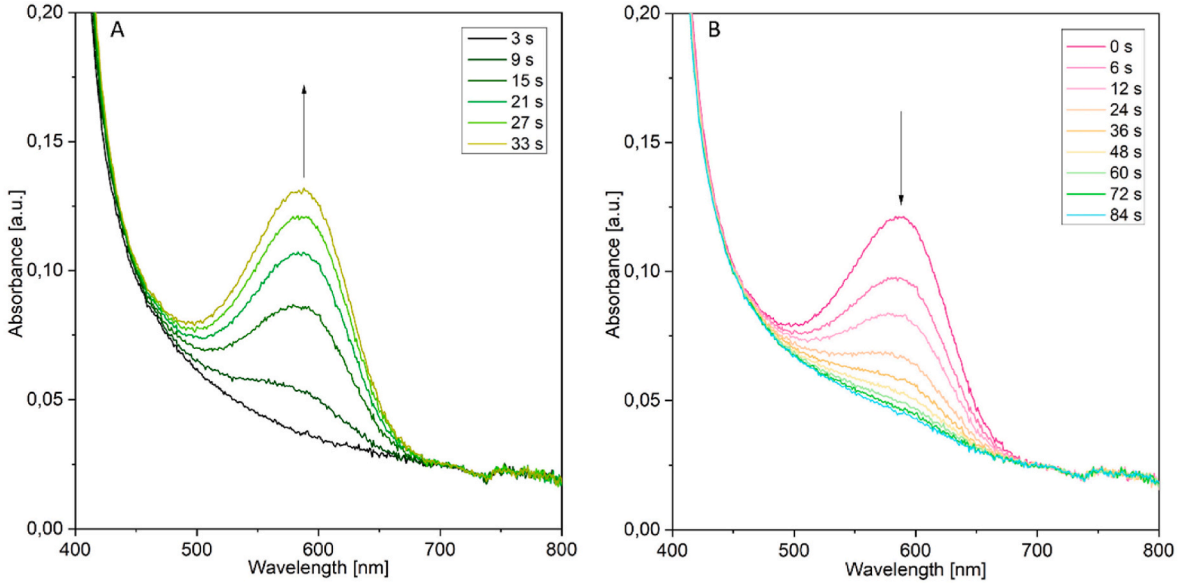

Fig. 3. A) UV-induced isomerization of spiropyrane to Vis-absorbing (active) merocyanine photoinitiator and B) thermal deactivation/isomerization of the active merocyanine photoinitiator to dormant spiropyrane species.

min using a UV-curing box (Asiga Flash Cure Box, Asiga, Japan).

2.3. Debinding, sintering

Thermal debinding was carried out simultaneously in vacuum according to the following temperature profile: room temperature to 500 °C at 0.5 °C/min, followed by a dwelling of 1h and cooling down to room temperature at 5 °C/min followed by a ramp to 800 °C at 1 °C/min and dwelling for 1h.

2.4. Particle, resin and specimen characterization

Particle Size Measurement were conducted at CeraNOVIS GmbH using DLS (Zetasizer, Malvern Instruments). UV–vis transmission measurement of the feedstock inside a single use cuvette was performed using a StellarNet Inc. BLACKComet C-50 spectrometer with a SL5 deuterium halogen light source. Additional measurements such as Absorption, were carried out with UV–vis spectrophotometer (Cary 50 Varian Inc./Agilent Technologies). Pictures of printed, debinded and sintered samples were taken using an optical microscope (VHX-7000, Keyence Corp.).

TGA-measurements were conducted using a TGA/DSC 3 + system (Mettler-Toledo S.p.A., Italy) at a heating rate of 10 °C/min^{-1}, in static air. X-ray diffraction (XRD 3000 PTS, Seifert now GE Inspection Technologies GmbH, Germany) was employed to investigate the phase assemblage.

3. Results and discussion

High transparency is the principal property that a ceramic photocurable resin must possess to enable its successful use in Xolography. Fig. 1A shows that the brownish YSZ-suspension, suitable for two-photon-polymerization, does not have sufficient transparency for Xolography. This can be related to the coloring effect of the 3 mol% yttria present. Though coloring results in absorption, and is, thus, a different physical effect than light scattering, technologically it has the same effect, as it attenuates the light intensity.

The most critical parameter for optimizing optical transparency is the particle size distribution of the ceramic material used. Fig. 2 reports the particle size distributions of the zirconia suspensions used to prepare the resins for 2PP and Xolography. It can be clearly seen that the standard yttria stabilized zirconia suspension (YSZ 5 nm), suitable for 2PP, had a particle size distribution with a significant fraction of particles larger than 50 nm and some particles even above 100 nm. Nevertheless, at small building envelopes of 0.1 mm^3 and at 800 nm operating wavelength for 2PP the transmittance is high enough to allow two-photon-excitation, despite the brownish color of the resin (see also Fig. 1A).

As a rule of thumb, particles should not exceed 1/10th of the wavelength used. Approximately 99.5 % of the YSZ particles were smaller than 80 nm (Fig. 2, red line), which leads to the assumption, that a very small fraction of particles (roughly 0.5 %) negatively affects the process by scattering the incoming light, but still allows for 2PP processing at 100–500 μm working distance and 750–800 nm wavelength.

For Xolography, operating at minimum 400 nm, approximately 3 % of particles are larger than 40 nm, causing too much scattering to successfully use the resin. On the contrary, the improved zirconia suspension with narrower particle size distribution (Fig. 2, black line) shows no significant particle fraction above 40 nm. Accordingly, the suspension and the related resin for Xolography reveal a high transparency in the relevant range of wavelengths.

To improve the optical properties of the photocurable resins, a zirconia suspension was specially tailored by CeraNovis GmbH, possessing an even narrower particle size distribution and almost no particles larger than 10 nm. Fig. 2B shows that the colorless, transparent suspension had a significantly increased transmission over the entire spectral range measured. The corresponding Xolography resins showed an exceptionally high transmittance at 10 mm path length, even higher than the original zirconia suspension used, compare Fig. 2B and C. Currently this effect is not fully understood, but a straightforward explanation is that the resin provides a better match between the refractive index of the ceramic particles $n_{zirconia} = 2.16$ [32] and the surrounding liquid phase, with refractive index of UDMA $n_{UDMA} = 1.48$ [33], while that of ethyl acetate is $n_{isopropanol} = 1.38$ [34].

Besides the optical properties, the chemical reactivity needs also to be appropriate for the Xolography requirements, meaning that any added chemical must not react with the photoinitiator prior to illumination. The change in the absorbance spectra during (Fig. 3A) and after illumination (Fig. 3B) shows that a fraction of dormant photoinitiator in its spiropyran form is converted during irradiation with UV light of 405 nm to the active visible light-absorbing merocyanine form, characterized by peak absorbance around 600 nm. In absence of a light stimulus,

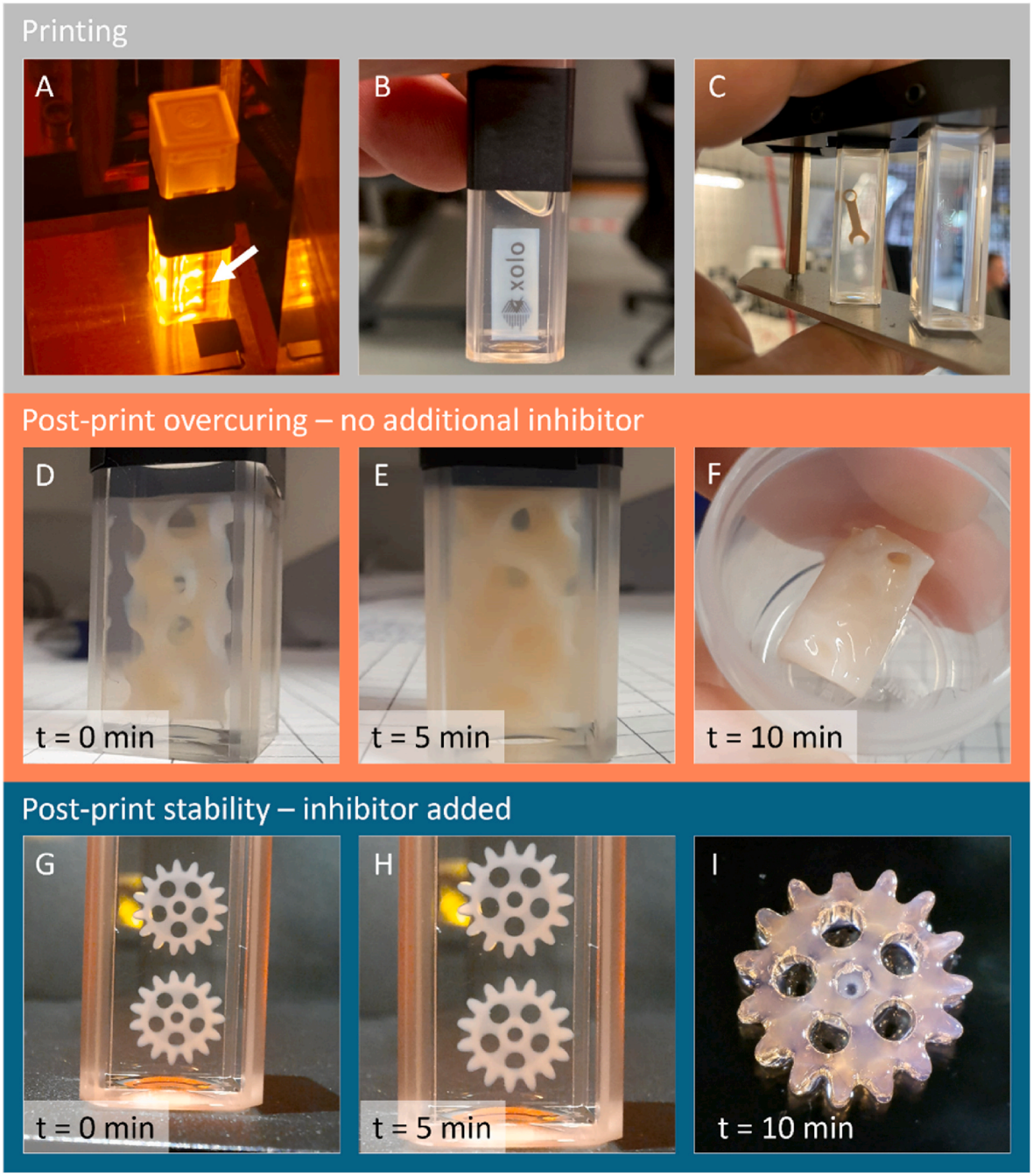

Fig. 4. Xolography printing with resin containing 70 wt% ZrO_2 nano-particles (5 nm) with narrow particle size distribution, A) active polymerization zone (UV light blade) as red line; B) Xolo logo printed and C) wrench printed inside the cuvettes; D) as printed part; E-F) post-print overcuring observable minutes after the printing until washing. (For interpretation of the references to color in this figure legend, the reader is referred to the Web version of this article.)

the photodynamic equilibrium reaction collapses and the so-formed merocyanine isomerizes thermally back to the dormant spiropyran form to completion.

The active photoinitiator is visible as a red fluorescent line in the cuvette (see arrow, Fig. 4A). The polymerization reaction results in opaque, whitish objects with the desired shape (Fig. 4B and C), proving that it was possible to devise formulations with enough transparency to enable photocuring deep within the volume of the resins. A typical print of 2–5 mm thickness takes only 3–7 min.

Specimens produced in the first trials showed good geometrical accuracy, but in a matter of minutes additional overpolymerization spontaneously occurred, e.g., filling the voids within the cellular structure (Fig. 4D) and could only be stopped by quick washing. Because of this effect, the resulting samples lost almost all of their geometrical fidelity (Fig. 4E–F). The origin of this phenomenon is yet unknown, but it might be connected to zirconia particles catalyzing the polymerization reaction [35,36] or causing some kind of phosphorescence or afterglow which can trigger the still activated photoinitiator [37]. The effect could be controlled utilizing an inhibitor (MEHQ), which captures unwanted radicals. However, the inhibitor concentration needs to be high enough to prevent unwanted post-printing curing, but also raises the threshold energy for the desired polymerization reaction. Higher UV energy is therefore needed for the printing process of ceramic loaded resins.

A more general observation of the Xolography process using resins filled with zirconia nanoparticles shows that the light-cured areas (Fig. 4B–D) and produced 3-dimensional specimen (Fig. 5A–C) appear

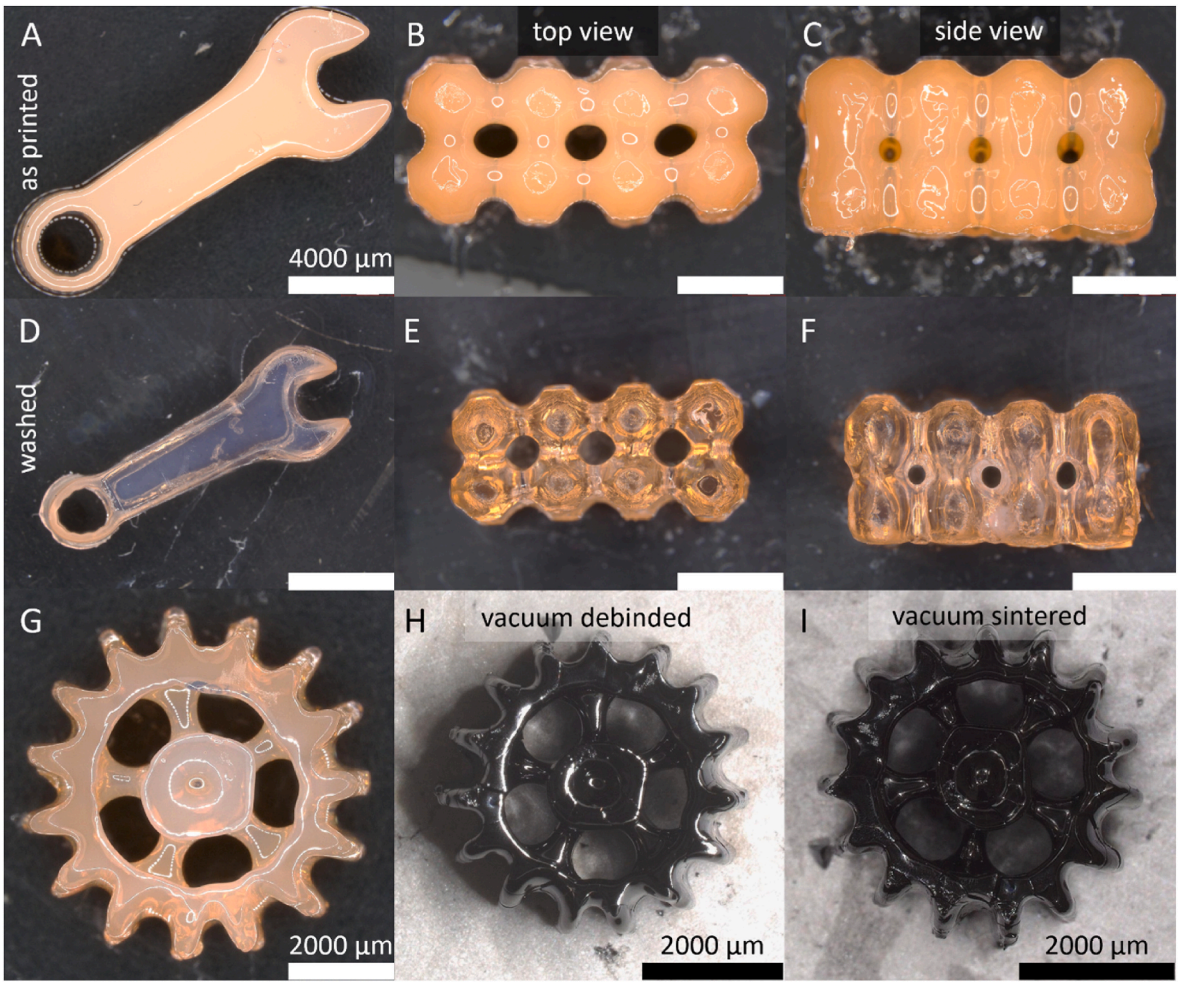

Fig. 5. Washed and post-cured opaque Xolography specimens of: A) wrench; B) 4 × 2 × 2 filled SchwarzP-structure from the top and C) the side. D-F) Once again washed and translucent specimens. (A-F have the same scale bar). G) as-printed gear wheel, H) vacuum-debinded and I) vacuum-sintered.

opaque or translucent. In other words, the starting material loses its transparency after it has been cross-linked. At present, this behavior is not fully understood, but the colorless white appearance of the cross-linked areas clearly indicate that light scattering is enhanced after crosslinking. This phenomenon is also observed for other particle-containing resins, e.g., silica nanoparticles or when co-monomers of different polarity polymerize. Phase separation during polymerization is very likely the cause for this phenomenon. It is known that photocurable resins tend to shrink as a result of crosslinking [38]. During Xolography printing, a UV beam is scanned across the x-z plane within the print envelope using a rotating mirror. Additionally, this plane is moved in the y-direction to address the entire print volume. The process is therefore quasi-continuous, but different positions in the volume are actually activated at different times. This discontinuous cross-linking might lead to an inhomogeneous density distribution within the cross-linked volume, which in turn would result in light scattering due to a modulation of the refractive index. After building up parts by the Xolography process and removal of excess resin by mild washing, a UV light soaking is generally performed to increase the degree of crosslinking within the part. Additional longer washing results into translucent specimens, which leads to the assumption that a washable compound, which is not covalently integrated into the polymer network, is the reason for the whitish appearance of printed parts. During crosslinking, the shrinkage and/or network formation of the mostly unpolar UDMA and ACMO might cause a local demixing, most probably of the polar dispersing agent TODS (3,6,9-Trioxadecane acid) and the co-initiator MDEA. Both are not directly involved in the network formation but cannot escape unless they are washed out (Fig. 5D–F). This viewpoint is supported by the observation, that the parts do shrink as a result of this additional washing, compare Fig. 5A–C and Fig. 4D–F.

The final post-printing steps to generate ceramic structures are constituted by the debinding and sintering, and they hold their own significant challenges. Besides the difficulty in successfully eliminating the gases deriving from the decomposition of the organic components within the samples without generating cracks, the phase transformation occurring in the un-stabilized tetragonal phase of zirconia, which tends to convert into the monoclinic phase with volume change, results in crack formation. Indeed, no crack-free parts could be obtained by conventional sintering. Vacuum-debinding (Fig. 5H) and Vacuum-sintering (Fig. 5I) leads to integer but still slightly cracked specimens. Most of the cracks are formed during debinding (up to 500 °C), as this is the process with the highest volume loss, accompanied by a linear shrinkage of 32 %. UDMA follows a rather complex decomposition pathway with 4 peaks in the differentiated TGA curve (DTG) (supplementary figure SF1). We assume UDMA decomposes gradually and therefore also loses its mechanical integrity during debinding, which complicates the formulation of the resin. Additional washing before the debinding increased the instability during debinding even more.

During Vacuum-sintering, the specimen shrunk another 3 % in length. The tetragonal to monoclinic zirconia phase transformation is suspected to cause further cracking at annealing to higher temperatures or switching to oxidizing sintering conditions. This has been confirmed by XRD analysis (see supplementary figure SF2). The as-received nanoparticles were mostly in the tetragonal phase. Due to the peak-

broadening, the orthorhombic [39] and cubic phases [40] might also be present. After sintering at 800 °C, monoclinic peaks appear at 33 and 36° [2 theta], showing evidence for the damaging t-m transformation during heating. Evidently, more work is required to successfully process the 3D printed samples into defect-free ceramic components.

4. Discussion

This preliminary investigation demonstrates the opportunities and challenges encountered when combining ceramic powder processing with volumetric additive manufacturing (specifically, Xolography).

4.1. Ceramic process chain and materials requirements

To produce technical ceramic parts, e.g., based on zirconia or yttria stabilized zirconia, using Xolography the process chain basically follows that of two-photon-polymerization (2PP) [18,19]. Nanoparticles are dispersed into a photocurable matrix (see Fig. 6) and an optimal mixture results in a transparent and photocurable resin which can be printed. After printing the three-dimensional object needs to be washed, debinded and sintered to obtain a ceramic part.

In order to be processable by Xolography, as well as to undergo subsequent debinding and sintering, the resin needs to possess the following characteristics.

- a high viscosity in the range of some Pa·s, to avoid movements of the part within the cuvette during printing and to retain the active polymerization zone in the desired region;
- photocurable by the Xolography process, and chemically compatible with xolo's proprietary dual-color photoinitiator;
- high transparency in the wavelength range from 400 to 800 nm, with an average free path penetration of at least 10 mm to enable printing within the volume;
- high solid loading of ceramic particles, ideally >70 wt%, to reduce shrinkage and the amount of organics to be decomposed during debinding. In the present study resins with up to 70 wt% content of zirconia particles were used, although successful volumetric printing has been reported for slurries with a lower loading, also [16].

4.2. Fulfilled and unfulfilled requirements

It was demonstrated that light scattering at the process relevant wavelengths within the volume of the ceramic filled resin could be reduced to an acceptable value when using a photocurable resin containing 70 wt% (30 vol%) of zirconia ceramic particles with a narrow particle size distribution (see Fig. 6).

While successfully completing this first, non-trivial step, three-dimensional objects with desired geometries and accuracy could be printed. The observed phenomenon of spontaneous over-polymerization in presence of zirconia nanoparticles could be suppressed by adding 4-methoxyphenol to the resin, but it needs to be better controlled and understood, and the formation of areas with different optical characteristics (translucent vs opaque) within the printed samples should be limited.

Additionally, we found that extracting the 3D printed parts from the viscous resin requires the formation of a sufficiently strong and stiff polymeric network within the parts. Furthermore, the washing procedure to remove uncured resin from the photocured parts is also a parameter that seemingly affects the geometrical definition and fidelity of the resulting parts. An in-depth analysis of the eluate after washing could reveal which chemical species are integrated into the polymeric network and which ones are not.

Finally, a better control of the debinding and, especially, of the phase transformation occurring in the tetragonal zirconia parts must be achieved before successfully completing the entire process chain transforming a photocurable feedstock into a 3D printed ZrO_2 part. A comprehensive thermal analysis of the resin would provide insights into the decomposition of all the different organic components and on the zirconia weight fraction.

The missing stabilization effect of yttria [41] certainly plays a major role in the unsuccessful attempt to obtain monolithic and crack-free zirconia ceramic structures. Due to the use of an extreme fine powder, their microstructure might differ from that of zirconia parts produced with other additive or even conventional manufacturing techniques, but regarding density and mechanical properties they should show comparable properties. In this context, the extent to which the coloration of the resin is affected by the addition of yttrium oxide will also need to be further clarified.

5. Conclusions

The present communication demonstrates, for the first time, the possibility of applying the Xolography linear volumetric printing technology to manufacture complex-shaped advanced ceramic green bodies following the classical powder processing route. The effect of light scattering on the ceramic (zirconia) particles in suspension was reduced

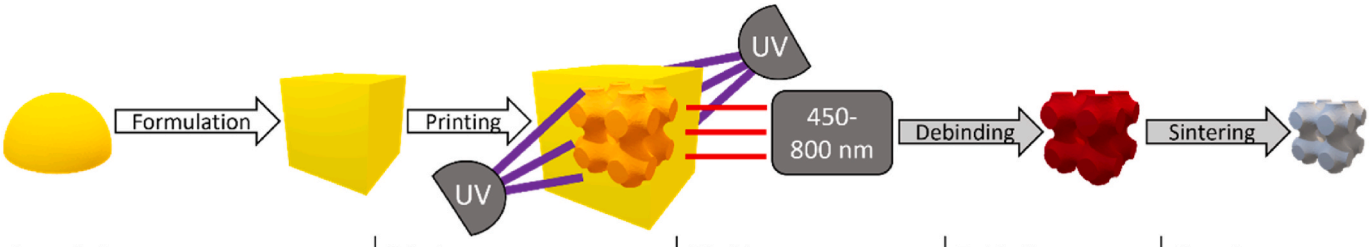

Formulation	Printing	Washing	Debinding	Sintering
☑ Zirconia (ZrO_2) as nanoparticles	☑ Transparency	☑ Residual resin		☑ Zirconia (ZrO_2)
☑ Photocurable matrix	☑ Hindered Post-curing	☑ UV-curing		
Compatible with:		☑ Reduced opacity		
☑ Photoinitiator and co-initiator				
☑ Dispersant				
☑ Inhibitor	☒ Opacity during curing	☒ Shrinkage	☒ Cracks	☒ Cracks
☑ Degassing agent		☒ Low stiffness	☒ UDMA decomposition	☒ No yttria stabilization

Fig. 6. Process chain starting from a nanoparticle suspension to resin, printing, debinding and sintering of 3-dimensional structures with Xolography. The table lists the challenges, which have or haven't been solved in this preliminary study.

to a negligible level by the use of extremely well-dispersed nanoparticles with a narrow, monomodal particle size distribution. The zirconia slurry mixed with two different photopolymers, at a solid loading of 70 wt% respectively 30 vol%, shows a high transparency allowing local cross-linking triggered by a dual color photoinitiator. Different 3D structures were successfully printed, washed, debinded and sintered to generate ceramic parts, however, still showing cracks. Debinding and sintering to non-cracked monolithic zirconia components still requires the addition of phase-stabilizing additives such as yttrium oxide, which, however, do not influence the optical properties of the resin in favour of its transparency. Further research effort is needed to better understand this phenomenon and find a suitable solution.

CRediT authorship contribution statement

J.C. Sänger: Conceptualization, Investigation, Methodology, Writing – original draft, Writing – review & editing. **N.F. König:** Investigation, Methodology, Resources, Validation, Visualization, Writing – original draft, Writing – review & editing. **A. De Marzi:** Data curation, Investigation. **A. Zocca:** Formal analysis, Supervision, Validation. **G. Franchin:** Supervision. **R. Bermejo:** Supervision, Funding acquisition. **P. Colombo:** Funding acquisition, Supervision, Writing – review & editing. **J. Günster:** Funding acquisition, Investigation, Resources, Supervision, Writing – review & editing.

Declaration of competing interest

The authors declare that they have no known competing financial interests or personal relationships that could have appeared to influence the work reported in this paper.

Acknowledgements

The authors thank Dr. rer. nat. Frank Meyer, CEO CeraNovis GmbH, for generously providing the material used in these experiments and Stefan Faber (CeraNovis GmbH) for the DLS-measurements and scientific support in discussions. The authors are grateful for funds provided by the Federal Institute of Materials Research and Testing (BAM). Johanna Sänger and Raul Bermejo acknowledge funding provided by the European Research Council (ERC) excellent science grant “CERATEXT” through the Horizon 2020 program under contract 817615.

This study was carried out within the MICS (Made in Italy – Circular and Sustainable) Extended Partnership and received funding from the European Union NextGenerationEU (PIANO NAZIONALE DI RIPRESA E RESILIENZA (PNRR) – MISSIONE 4 COMPONENTE 2, INVESTIMENTO 1.3 – D.D. 1551.11-10-2022, PE00000004). This manuscript reflects only the authors’ views and opinions, neither the European Union nor the European Commission can be considered responsible for them.

Appendix A. Supplementary data

Supplementary data to this article can be found online at https://doi.org/10.1016/j.oceram.2024.100655.

References

[1] A. Zocca, P. Colombo, C.M. Gomes, J. Günster, Additive manufacturing of ceramics: issues, potentialities, and opportunities, J. Am. Ceram. Soc. 98 (7) (2015) 1983–2001, https://doi.org/10.1111/jace.13700.
[2] M.L. Griffith, J.W. Halloran, Ultraviolet curing of highly loaded ceramic suspensions for stereolithography of ceramics, in: Proc. Solid Freeform Fabrication Symp, DTIC Document, 1994, pp. 396–403.
[3] M.L. Griffith, J.W. Halloran, Freeform fabrication of ceramics via stereolithography, J. Am. Ceram. Soc. 79 (10) (1996) 2601–2608, https://doi.org/10.1111/j.1151-2916.1996.tb09022.x.
[4] C. Hinczewski, S. Corbel, T. Chartier, Ceramic suspensions suitable for stereolithography, J. Eur. Ceram. Soc. 18 (6) (1998) 583–590, https://doi.org/10.1016/S0955-2219(97)00186-6.
[5] S. Kirihara, T. Niki, Three-dimensional stereolithography of alumina photonic crystals for terahertz wave localization, Int. J. Appl. Ceram. Technol. 12 (1) (2015) 32–37, https://doi.org/10.1111/ijac.12320.
[6] T. Chartier, et al., Fabrication of millimeter wave components via ceramic stereo- and microstereolithography processes, J. Am. Ceram. Soc. 91 (8) (2008) 2469–2474, https://doi.org/10.1111/j.1551-2916.2008.02482.x.
[7] N. Delhote, D. Baillargeat, S. Verdeyme, C. Delage, C. Chaput, Narrow ka bandpass filters made of high permittivity ceramic by layer-by-layer polymer stereolithography, in: 2006 European Microwave Conference, 2006, pp. 510–513, https://doi.org/10.1109/EUMC.2006.281422, 10-15 Sept. 2006.
[8] N. Delhote, D. Baillargeat, S. Verdeyme, C. Delage, C. Chaput, Ceramic layer-by-layer stereolithography for the manufacturing of 3-D millimeter-wave filters, IEEE Trans. Microw. Theor. Tech. 55 (3) (2007) 548–554, https://doi.org/10.1109/TMTT.2007.891690.
[9] S.C. Ventura, et al., A new SFF process for functional ceramic components, in: Solid Freeform Fabrication Symposium Proceedings, 1996, pp. 318–325.
[10] M. Schwentenwein, P. Schneider, J. Homa, Lithography-based ceramic manufacturing: a novel technique for additive manufacturing of high-performance ceramics, in: Advances in Science and Technology, vol. 88, Trans Tech Publ, 2014, pp. 60–64. https://doi.org/10.4028/www.scientific.net/AST.88.60.
[11] V. Tomeckova, J.W. Halloran, Cure depth for photopolymerization of ceramic suspensions, J. Eur. Ceram. Soc. 30 (15) (2010) 3023–3033, https://doi.org/10.1016/j.jeurceramsoc.2010.06.004.
[12] V. Tomeckova, J.W. Halloran, Flow behavior of polymerizable ceramic suspensions as function of ceramic volume fraction and temperature, J. Eur. Ceram. Soc. 31 (14) (2011) 2535–2542, https://doi.org/10.1016/j.jeurceramsoc.2011.01.019.
[13] M. Staudacher, T. Lube, J. Glettler, U. Scheithauer, M. Schwentenwein, A novel test specimen for strength testing of ceramics for additive manufacturing, Open Ceramics 15 (2023) 100410, https://doi.org/10.1016/j.oceram.2023.100410, 2023/09/01.
[14] T. Lube, M. Staudacher, A.-K. Hofer, J. Schlacher, R. Bermejo, Stereolithographic 3D printing of ceramics: challenges and opportunities for structural integrity, Adv. Eng. Mater. (2022) 2200520, https://doi.org/10.1002/adem.202200520 n/a, no. n/a.
[15] K. Huang, G. Franchin, and P. Colombo, "Volumetric Additive Manufacturing of SiOC by Xolography," Small, vol. n/a, no. n/a, p. 2402356, doi: https://doi.org/10.1002/smll.202402356.
[16] L. A. Myers, J. J. Schwartz, M. P. De Beer, R. L. Walton, and D. H. Porcincula, "Development of transparent, particle-loaded photoresins for volumetric additive manufacturing of silica glass," J. Polym. Sci., vol. n/a, no. n/a, doi: https://doi.org/10.1002/pol.20230654.
[17] J.T. Toombs, et al., Volumetric additive manufacturing of silica glass with microscale computed axial lithography, Science 376 (6590) (2022) 308–312, https://doi.org/10.1126/science.abm6459.
[18] J.C. Sänger, B.R. Pauw, H. Sturm, J. Günster, First time additively manufactured advanced ceramics by using two-photon polymerization for powder processing, Open Ceramics (2020) 100040, https://doi.org/10.1016/j.oceram.2020.100040, 2020/12/03/.
[19] J.C. Sänger, et al., Entering a new dimension in powder processing for advanced ceramics shaping, Adv. Mater. (2022) 2208653, https://doi.org/10.1002/adma.202208653 n/a, no. n/a.
[20] A. Lale, et al., Holographic photopolymerization combined to microfluidics for the fabrication of lab-in-lab microdevices and complex 3D micro-objects, Heliyon 9 (9) (2023) e20054, https://doi.org/10.1016/j.heliyon.2023.e20054, 2023/09/01/.
[21] M. Regehly, et al., Xolography for linear volumetric 3D printing, Nature 588 (7839) (2020) 620–624, https://doi.org/10.1038/s41586-020-3029-7, 2020/12/01.
[22] L. Stüwe, et al., Continuous volumetric 3D printing: Xolography in flow, Adv. Mater. 36 (4) (2024) 2306716, https://doi.org/10.1002/adma.202306716.
[23] N. Corrigan, X. Li, J. Zhang, and C. Boyer, "Xolography for the Production of Polymeric Multimaterials," Advanced Materials Technologies, vol. n/a, no. n/a, p. 2400162, doi: https://doi.org/10.1002/admt.202400162.
[24] G.C. Wei, Transparent ceramic lamp envelope materials, J. Phys. Appl. Phys. 38 (17) (2005) 3057, https://doi.org/10.1088/0022-3727/38/17/S07, 2005/08/19.
[25] G. Witz, V. Shklover, W. Steurer, S. Bachegowda, H.-P. Bossmann, Phase evolution in yttria-stabilized zirconia thermal barrier coatings studied by rietveld refinement of X-ray powder diffraction patterns, J. Am. Ceram. Soc. 90 (9) (2007) 2935–2940, https://doi.org/10.1111/j.1551-2916.2007.01785.x.
[26] C.F. Bohren, Multiple scattering of light and some of its observable consequences, Am. J. Phys. 55 (6) (1987) 524–533, https://doi.org/10.1119/1.15109.
[27] A.A. Kokhanovsky, On light scattering in random media with large densely packed particles, J. Geophys. Res. Atmos. 103 (D6) (1998) 6089–6096, https://doi.org/10.1029/97JD03632.
[28] D.A. Wright, J.S. Thorp, A. Aypar, H.P. Buckley, Optical absorption in current-blackened yttria-stabilized zirconia, J. Mater. Sci. 8 (6) (1973) 876–882, https://doi.org/10.1007/BF02397918, 1973/06/01.
[29] N.T. Melamed, Optical properties of powders. Part I. Optical absorption coefficients and the absolute value of the diffuse reflectance. Part II. Properties of luminescent powders, J. Appl. Phys. 34 (3) (2004) 560–570, https://doi.org/10.1063/1.1729309.
[30] J.A. Adam, The mathematical physics of rainbows and glories, Phys. Rep. 356 (4) (2002) 229–365, https://doi.org/10.1016/S0370-1573(01)00076-X, 2002/01/01/.
[31] J. Joo, et al., Multigram scale synthesis and characterization of monodisperse tetragonal zirconia nanocrystals, J. Am. Chem. Soc. 125 (21) (2003) 6553–6557, https://doi.org/10.1021/ja034258b, 2003/05/01.

[32] D.L. Wood, K. Nassau, Refractive index of cubic zirconia stabilized with yttria, Appl Optics 21 (16) (1982) 2978–2981, https://doi.org/10.1364/AO.21.002978, 1982/08/15.
[33] K. Yoshinaga, K. Yoshihara, Y. Yoshida, Development of new diacrylate monomers as substitutes for Bis-GMA and UDMA, Dent. Mater. 37 (6) (2021) e391–e398, https://doi.org/10.1016/j.dental.2021.02.023, 2021/06/01/.
[34] Y.-C. Kao, C.-H. Tu, Densities, viscosities, refractive indices, and surface tensions for binary and ternary mixtures of 2-propanol, tetrahydropyran, and 2,2,4-trimethylpentane, J. Chem. Therm. 43 (2) (2011) 216–226, https://doi.org/10.1016/j.jct.2010.08.019, 2011/02/01/.
[35] G. Pacchioni, Role of nanostructuring on the properties of oxide materials: the case of zirconia nanoparticles, Eur. J. Inorg. Chem. 2019 (6) (2019) 751–761, https://doi.org/10.1002/ejic.201801314.
[36] A.R. Puigdollers, F. Illas, G. Pacchioni, Structure and properties of zirconia nanoparticles from density functional theory calculations, J. Phys. Chem. C 120 (8) (2016) 4392–4402, https://doi.org/10.1021/acs.jpcc.5b12185, 2016/03/03.
[37] L. Puust, V. Kiisk, K. Utt, H. Mändar, I. Sildos, Afterglow and thermoluminescence of ZrO2 nanopowders, Cent. Eur. J. Phys. 12 (6) (2014) 415–420, https://doi.org/10.2478/s11534-014-0456-9, 2014/06/01.
[38] H. Fang, C.A. Guymon, Recent advances to decrease shrinkage stress and enhance mechanical properties in free radical polymerization: a review, Polym. Int. 71 (5) (2022) 596–607, https://doi.org/10.1002/pi.6341.
[39] S. Liu, et al., Metastable adaptive orthorhombic martensite in zirconia nanoparticles, J. Appl. Crystallogr. 47 (2) (2014) 684–691, https://doi.org/10.1107/S1600576714003331.
[40] A. Behbahani, S. Rowshanzamir, A. Esmaeilifar, Hydrothermal synthesis of zirconia nanoparticles from commercial zirconia, Procedia Eng. 42 (2012) 908–917, https://doi.org/10.1016/j.proeng.2012.07.483, 2012/01/01/.
[41] A. Karthik, et al., Stabilization of tetragonal zirconia in alumina-zirconia and alumina-yttria stabilized zirconia nanocomposites: a comparative structural analysis, Mater. Char. 158 (2019) 109964, https://doi.org/10.1016/j.matchar.2019.109964, 2019/12/01/.